Air inequality: Global divergence in urban fine particulate matter trends

Joshua S. Apte[1,2]*, Sarah Seraj[3], Sarah E. Chambliss[3], Melanie Hammer[4,5], Veronica A. Southerland[6], Susan C. Anenberg[6], Aaron van Donkelaar[5], Michael Brauer[7,8], Randall V. Martin[4,5]

[1]Department of Civil and Environmental Engineering, University of California, Berkeley, USA
[2]School of Public Health, University of California, Berkeley, USA
[3] Department of Civil, Architectural and Environmental Engineering, University of Texas at Austin, Austin, TX USA
[4]Department of Energy, Environmental and Chemical Engineering, Washington University, St. Louis, MO, USA
[5]Department of Physics, Dalhousie University, Halifax, Canada
[6]School of Public Health, George Washington University, Washington, DC, USA
[7]School of Population and Public Health, The University of British Columbia, Vancouver BC, Canada
[8]Institute for Health Metrics and Evaluation, University of Washington, Seattle WA, USA
* Correspondence to apte@berkeley.edu.

Fine particle air pollution ($PM_{2.5}$) is the largest global environmental risk factor for ill-health and is implicated in >7% of all human deaths.[1-3] Improved air quality is a key policy goal for cities, yet in-situ $PM_{2.5}$ measurements are missing[4] for >50% of the world's urban population. Here, we apply satellite remote sensing to develop a 21-year time series of ground-level $PM_{2.5}$ concentrations for the 4231 urban areas with populations >100,000 (2.9 billion people) from 1998 -2018. Globally, we find the most polluted cities are generally small (<1 million population) and lack $PM_{2.5}$ monitors. Since 1998, we observe a growing divide in urban air quality between cities in lower and higher-income regions, with the $PM_{2.5}$ disparity increasing by >50% (from 25 to 39 µg m^{-3}) between the highest- and lowest income quartiles of world cities. Within Asia, a sharp divergence is underway, with sustained $PM_{2.5}$ increases in South Asian cities (+48%) contrasted against dramatic improvements in Chinese cities (-40% since 2011). While 85% of the world's urban population experiences $PM_{2.5}$ higher than World Health Organization guidelines, urban $PM_{2.5}$ concentrations are tightly linked to regional conditions, suggesting that city-level efforts alone may be insufficient to address this major health threat.

Urban air pollution has been a concern for human health and welfare since the dawn of the industrial era,[5,6] and a major focus of modern environmental policy in countries around the world for the past 70 years. Fine particulate matter ($PM_{2.5}$) contributes >90% of the burden of disease attributed to ambient air pollution,[2] or approximately 4-7 million premature deaths globally[1,2,7] shortening the average human life by ~1 year.[8] Despite the major public health burden of $PM_{2.5}$, careful assessment of global urban air quality trends has been hampered by the general absence of an observational record for most cities on the planet.[4,9] As of 2018, approximately 1.5 billion people lived in ~2800 world cities with more than 100,000 people but with no valid, continuous $PM_{2.5}$ measurements[10] (Extended Data Figure 1). Regions with especially few $PM_{2.5}$ monitors include large parts of Asia, Africa, and South America, where $PM_{2.5}$ concentrations are estimated to be especially high and changing rapidly.[4] Here, we develop a time-series of urban $PM_{2.5}$ estimates for each of the 4,231 worldwide urban agglomerations[11,12] with more than 100,000 inhabitants (2.9 billion people in 2018), which account for ~69% of the world's overall urban population and 38 % of the global population. Our dataset encompasses the period from 1998 to 2018, when the world's urban population[13] increased by 56% from 2.7 billion (46% of the total human population) to 4.2 billion (56%), including a doubling of the urban population in Asia to 2.3 billion people.

Urban $PM_{2.5}$ dataset: global and regional patterns

As described in Methods, we use a high-resolution ($0.01^o \times 0.01^o$, ~ 1 km^2) $PM_{2.5}$ dataset[14] based on satellite remote sensing of aerosol optical depth[15] (AOD) to develop annual-average urban-level $PM_{2.5}$ estimates for 4231 urban areas during the years 1998-2018 (Extended Data Figure 2). For the ~1000 cities (~5000 city-years, ~12000 monitor-years) with valid in-situ $PM_{2.5}$ measurements over this period, model performance is excellent, estimating measured annual-

55 average $PM_{2.5}$ with $R^2 = 0.91$, slope = 0.91, and mean absolute error of 3.6 μg m^{-3} (16%,
56 Extended Data Figure 3). For 2018, the population-weighted mean (PWM) urban $PM_{2.5}$
57 concentration in our dataset was 31.3 μg m^{-3}. Overall, 84% of the urban population lived in 3504
58 cities where concentrations exceeded the annual-average World Health Organization (WHO) air
59 quality guideline of 10 μg m^{-3} $PM_{2.5}$, and 35% of the urban population lived in cities where
60 $PM_{2.5}$ exceeds the WHO interim target of 35 μg m^{-3}.
61 For year 2018, the highest urban $PM_{2.5}$ concentrations were in South Asia, China, and West
62 Africa, while many of the world's least polluted cities were in North America, Brazil, and parts
63 of Europe. Considering the 400 (~10% of) cities with the highest $PM_{2.5}$ concentrations in 2018,
64 annual-average concentrations ranged from 62-165 μg m^{-3} (PWM: 85 μg m^{-3}, Extended Data
65 Figure 4). These most polluted cities were predominantly in India (50%), elsewhere in South
66 Asia (15%), Nigeria (17%), and China (11%). This group included 14 cities with more than 3
67 million people, including Delhi, Kolkata and Lucknow (India); Karachi (Pakistan); Dhaka
68 (Bangladesh); Accra (Ghana), Lagos and Kano (Nigeria); and Lima (Peru). However, the
69 majority of the world's most polluted cities have populations less than 1 million, and only 20%
70 of these cities in the upper concentration decile have valid in-situ $PM_{2.5}$ measurement data. This
71 finding stands in contrast to previous literature about the world's most polluted cities,[16] which
72 tends to emphasize larger and more prominent urban areas that have more extensive in-situ
73 monitoring.[4,17]

74 ## Regional divergence in $PM_{2.5}$ trends

75 Trend analyses for $PM_{2.5}$ over the period of 1998-2018 paint a picture of a highly dynamic
76 evolution in urban air pollution around the world (Figure 1, Extended Data Figure 5). While a
77 single linear or exponential trend provides an incomplete summary of the complex dynamics of

urban air pollution over two decades, 81% of the global urban population experienced statistically significant upwards or downwards trends in $PM_{2.5}$.

Our data reveal sharp global divergence in urban $PM_{2.5}$ over the past two decades. Key results from best-fit concentration trends for the full two-decade period are evident in Figure 1a: ~2% yr^{-1} reductions in $PM_{2.5}$ in the Eastern US, Mexico, and Western Europe, and 1-3% yr^{-1} increases in $PM_{2.5}$ in South and Southeast Asia, the Middle East, and parts of South America and East Africa. For most sub-Saharan African cities, evidence of a trend is obscured by large (±5-10 μg m^{-3}) interannual variability caused by episodic regional smoke and dust transport.[18] Notable counterexamples to broader regional trends include $PM_{2.5}$ reductions in Colombian and coastal Brazilian cities contrasting with increases elsewhere in South America, and $PM_{2.5}$ increases since 2008 in smaller cities in the Western U.S. and Canada owing to the influence of wildfire smoke.

The divergent air pollution trends within Asia are shown in Figure 1b-c and Figure 2. Strong upward concentration trends tracked closely for Chinese and South Asian cities from 1998-2011 (Figure 2a). In 2011, median $PM_{2.5}$ concentrations were virtually identical for Chinese and South Asian cities. However, since 2011, nearly all major cities in China experienced sustained and precipitous declines in $PM_{2.5}$ of 15-30 μg m^{-3} (-7% yr^{-1}), with more than 85% of Chinese cities experiencing lower $PM_{2.5}$ in 2018 than in 1998. This trend, as documented elsewhere,[19-22] resulted from an extensive combination of energy and air pollution control policies enacted after 2011. Over the same period, upward trends in $PM_{2.5}$ (~2% yr^{-1}) persisted in South Asian cities, such that by 2018, the 25th percentile $PM_{2.5}$ concentration in South Asian cities (48 μg m^{-3}) exceeded the 75th percentile in Chinese cities (45 μg m^{-3}). Reflecting the large-scale exodus of Chinese cities from the ranks of the world's most polluted, of the world's 25 most polluted cities for $PM_{2.5}$, 21 were in China in 1998, while 22 were in India in 2018 (Extended Data Figure 4).

Conversely, since 2008, urban $PM_{2.5}$ grew most rapidly in South Asia, accounting for more than 90% of cities worldwide that experienced increases greater than 0.5 $\mu g\ m^{-3}\ y^{-1}$. Notably, the most rapid increases in $PM_{2.5}$ in India were not in the heavily polluted cities of the Indo-Gangetic Plain,[23] but rather in the less-polluted southern cities (Figure 1c), including Pune and Bangalore, which have become major economic hubs.

We find a growing divide in urban $PM_{2.5}$ concentrations between lower and higher-income countries over the past two decades (Figure 2). In 1998, the global distribution of urban $PM_{2.5}$ was essentially unimodal with respect to the urban population. At that time, there was substantial overlap in the concentration distributions of lower- and higher-income countries: relatively polluted cities in the United States or Western Europe had similar $PM_{2.5}$ levels to comparatively clean Indian or Chinese cities (Figure 2b). By 2011, concentrations had diverged sharply between the higher- and lower-income countries, such that the global distribution of urban $PM_{2.5}$ became distinctly bimodal (Figure 2b), removing nearly all overlap in the urban $PM_{2.5}$ distributions in the high- and low-income world. Notable changes between 1998 and 2011 (compare Fig 2b-c) include a large upward shift in the concentration distribution for already-polluted Asian countries, resulting in a 70% increase in the urban population at $PM_{2.5} > 35\ \mu g\ m^{-3}$; a large increase in the urban population living at $PM_{2.5} < 10\ \mu g\ m^{-3}$; and steep declines in $PM_{2.5}$ concentrations in Mexico and Central America. Between 2011 and 2018, the storyline becomes more complex, as the unprecedented $PM_{2.5}$ improvements in China (Figure 2a) stand out as a clear exception to the continued global trend towards increasingly unequal urban air pollution. From 2011-2018, the share of China's urban population meeting the national $PM_{2.5}$ standard ($< 35\ \mu g\ m^{-3}$) quadrupled from 9% to 38%, resulting in a broad – but again unimodal – global urban $PM_{2.5}$ distribution (Figure 2d). Excluding Chinese cities from the visualization

(Figure 2e-f) accentuates the increasing global divergence in urban air quality between the high-income countries and the 5 largest low-income countries (India, Indonesia, Bangladesh, Pakistan and Nigeria). Figure 2a highlights two equal city population groups corresponding to the lowest and highest national income quartiles (Q1 and Q4). On a PWM basis, the concentration disparity in urban $PM_{2.5}$ among these lowest and highest income groupings grew by more than 50% from 1998 to 2018. Average concentrations in the low-income Q1 cities grew from 45 to 54 $\mu g\ m^{-3}$, while average urban $PM_{2.5}$ declined from 20 to 15 μg^{-3} for cities in high-income Q4 over the same period. In sum, these data point to continued urban $PM_{2.5}$ improvements in higher-income countries, exceptional recent progress in China, and a sustained deterioration of urban air quality in many of the world's lower income countries.

Urban $PM_{2.5}$ is influenced by regional conditions

We explore here how $PM_{2.5}$ concentrations in the world's cities relate to their surroundings. Three key considerations are relevant. First, $PM_{2.5}$ sources are distributed across the entire urban-to-rural landscape. Many key emitters of $PM_{2.5}$ and its precursors are found at the urban periphery or in rural areas, including electric power generation, domestic fuel combustion, some types of industry, agriculture, and fires. Second, $PM_{2.5}$ consists of both primary particles (which local sources may strongly influence) and of secondary organic and inorganic material (for which regional emissions and atmospheric chemistry play a decisive role). In most urban areas, secondary particle mass typically exceeds primary particle mass.[24,25] Characteristic atmospheric reaction and transport timescales of hours to days impose a spatially diffuse footprint for secondary $PM_{2.5}$.[26,27] Third, cities influence their surroundings, as "urban plumes" elevate $PM_{2.5}$ concentrations in downwind areas.[28,29]

146 We characterize here the relationship between urban and regional concentrations using high-
147 resolution 1-km $PM_{2.5}$ data by computing isotropic (directionless) concentration decay profiles
148 away from the center of each city in the dataset (see Methods). Figure 3a illustrates how, on
149 average, concentrations decrease moving away from the city center for cities of all sizes, with
150 increasingly strong decay patterns for cities of increasing size. The urban increment in $PM_{2.5}$
151 relative to regional surroundings is generally modest and reflects the regional nature of $PM_{2.5}$ and
152 the importance of secondary formation. Considering the decrease in concentration out to 300 km
153 from a city center, average $PM_{2.5}$ concentrations decay by 12% for smaller cities sized 100-400k
154 (~25% of urban population), and by 30% for the world's largest cities with > 5.6 M inhabitants
155 (~25% of urban population). These patterns are similar for cities in both cleaner and more
156 polluted regions, and are robust to the specific year analyzed.
157 Relative to smaller cities, larger cities are both somewhat more polluted, and have $PM_{2.5}$
158 concentrations that are more elevated relative to regional background. However, the effect is
159 subtle. Figure 3b presents the ratio of city-center to 300-km radius concentrations as a function
160 of city population. Cities in the highest population bin in Figure 3b have $PM_{2.5}$ levels that are on
161 average only 50% greater than their regional surroundings. Globally, there is little association
162 between city population and $PM_{2.5}$ ($r = 0.03$). The half of the world's urban population living in
163 the larger cities (population ≥ 1.6 M) experiences $PM_{2.5}$ levels only moderately elevated relative
164 to smaller cities (crude and regionally-adjusted differences: 1.9 and 1.8 $\mu g\ m^{-3}$).
165 Over the past 40 years, there has been extensive scientific emphasis on poor air quality in
166 megacities, [30-33] which we consider here as the 39 global agglomerations with population of more
167 than 10 million (~600 M inhabitants in 2018). While some megacities are notorious for air
168 pollution extremes, we find that globally, megacities have annual-average $PM_{2.5}$ (PWM: 37 μg

169 m^{-3}) that is only moderately elevated (3-4 μg m^{-3}, ~10-20%) relative to non-megacities in their
170 regions. These findings imply that the traditional emphasis on heavily polluted megacities may
171 be an example of an observational bias (the "streetlight effect"): attention gravitates to those
172 larger cities that have available monitoring data.

173 Temporal trends in $PM_{2.5}$ concentrations tend to be broadly similar for cities and their
174 regional surroundings. For more than 80% of all cities, we find high time-series correlation ($r >$
175 0.8) between urban $PM_{2.5}$ and concentrations in surrounding 100-300 km regions. This result is
176 consistent with the practice of air quality management in the U.S., China, and Europe, where
177 regional strategies have been used in conjunction with city measures to improve urban air
178 quality. Two key ingredients to these strategies have included controlling regional emissions
179 sources (e.g., power generation, rural household solid fuel use) and reducing secondary aerosol
180 precursor emissions (e.g., SO_2 from coal use) [19,22,34,35] In combination, our findings emphasize
181 how past and future trends in urban $PM_{2.5}$ require consideration of the broader context of
182 regional sources and atmospheric processes.

183 By overcoming major global data gaps in the in-situ observational record, we find a clear
184 picture of global divergence in urban $PM_{2.5}$, with increasing "air inequality" for $PM_{2.5}$ between
185 cities in lower- and higher-income countries. Prior theoretical and empirical scholarship has
186 described inconsistent relationships between economic development and local environmental
187 quality.[7,36-38] Policy choices also matter. Across a diverse range of economic conditions, a
188 common theme for notable reductions in urban $PM_{2.5}$ is the role of strong policy
189 measures.[19,22,31,39,40] The striking contrast between unprecedentedly rapid $PM_{2.5}$ reductions in
190 Chinese cities and increasingly severe urban air pollution in South Asia illustrates how
191 comprehensive policy efforts can sharply redirect air pollution trends even while sustaining rapid

economic expansion. Still, roughly a billion people in mostly lower-income countries reside in cities with increasing $PM_{2.5}$. Several high-profile global and national environmental policy efforts focus on city-led actions,[41-44] often emphasizing the strong co-benefits between greenhouse gas emissions reduction and improvements in localized air pollutants. Our findings, however, emphasize how urban $PM_{2.5}$ is tightly coupled to surrounding conditions, suggesting that coordinated regional or national policies [e.g., 45,46] may also be needed to bring cleaner air to an increasingly urbanized world. These data use a consistent methodology which, with future updates, will help track the effectiveness of air quality management actions at regional, national and city levels.

References

1 Burnett, R. *et al.* Global estimates of mortality associated with long-term exposure to outdoor fine particulate matter. *Proc. Natl. Acad. Sci.* **115**, 9592 (2018).

2 Cohen, A. J. *et al.* Estimates and 25-year trends of the global burden of disease attributable to ambient air pollution: an analysis of data from the Global Burden of Diseases Study 2015. *The Lancet* **389**, 1907-1918 (2017).

3 Apte, J. S., Marshall, J. D., Brauer, M. & Cohen, A. J. Addressing global mortality from ambient $PM_{2.5}$. *Environ. Sci. Technol.* **49**, 8057–8066 (2015).

4 Martin, R. V. *et al.* No one knows which city has the highest concentration of fine particulate matter. *Atmos. Env. X* **3**, 100040 (2019).

5 Brimblecombe, P. London air pollution, 1500-1900. *Atmospheric Environment (1967)* **11**, 1157-1162 (1977).

6 Evelyn, J. *Fumifugium: The Inconveniencie of the aer and smoak of London*. (1661).

7 Murray, C. J. L. *et al.* Global burden of 87 risk factors in 204 countries and territories, 1990-2019: a systematic analysis for the Global Burden of Disease Study 2019. *The Lancet* **396**, 1223-1249 (2020).

8 Apte, J. S., Brauer, M., Cohen, A. J., Ezzati, M. & Pope, C. A. Ambient $PM_{2.5}$ reduces global and regional life expectancy. *Environmental Science & Technology Letters* **5**, 546-551 (2018).

9 Carvalho, H. The air we breathe: differentials in global air quality monitoring. *The Lancet Respiratory Medicine* **4**, 603-605.

10 World Health Organization. *WHO Global Ambient Air Quality Database (Update 2020)*. (WHO, 2020).

11 Angel, S. *et al.* Atlas of urban expansion—2016 edition. *Areas and densities. Cambridge, MA: NYU Urban Expansion Program at New York University, UN-Habitat, and the Lincoln Institute of Land Policy* (2016).

12 Angel, S., Parent, J., Civco, D. L., Blei, A. & Potere, D. The dimensions of global urban expansion: Estimates and projections for all countries, 2000-2050. *Prog. Plann.* **75**, 53-107 (2011).
13 United Nations; Department of Economic and Social Affairs; Population Division. *World Urbanization Prospects: The 2018 Revision*. (2018).
14 Hammer, M. S. *et al.* Global estimates and long-term trends of fine particulate matter concentrations (1998–2018). *Environ. Sci. Technol.* **54**, 7879-7890 (2020).
15 van Donkelaar, A. *et al.* Global estimates of ambient fine particulate matter concentrations from satellite-based aerosol optical depth: development and application. *Environ. Health Persp.* **118**, 847-855 (2010).
16 Schwela, D. H. & Haq, G. Strengths and weaknesses of the WHO Urban Air Pollutant Database. *Aerosol Air Qual. Res.* **20**, 1026-1037 (2020).
17 Chow, J. C. *et al.* Megacities and atmospheric pollution. *J. Air Waste Manage. Assoc.* **54**, 1226-1235 (2004).
18 Swap, R., Ulanski, S., Cobbett, M. & Garstang, M. Temporal and spatial characteristics of Saharan dust outbreaks. *J. Geophys. Res. Atmos.* **101**, 4205-4220 (1996).
19 Ma, Z., Liu, R., Liu, Y. & Bi, J. Effects of air pollution control policies on $PM_{2.5}$ pollution improvement in China from 2005 to 2017: a satellite-based perspective. *Atmos. Chem. Phys.* **19**, 6861-6877 (2019).
20 Zhai, S. *et al.* Fine particulate matter ($PM_{2.5}$) trends in China, 2013–2018: separating contributions from anthropogenic emissions and meteorology. *Atmos. Chem. Phys.* **19**, 11031-11041 (2019).
21 Xiao, Q. *et al.* Changes in spatial patterns of $PM_{2.5}$ pollution in China 2000–2018: Impact of clean air policies. *Environ. Int.* **141**, 105776 (2020).
22 Zhang, Q. *et al.* Drivers of improved $PM_{2.5}$ air quality in China from 2013 to 2017. *Proc. Natl. Acad. Sci.* **116**, 24463-24469 (2019).
23 Apte, J. S. & Pant, P. Toward cleaner air for a billion Indians. *Proc. Natl. Acad. Sci.* **116**, 10614 (2019).
24 Zhang, Q. *et al.* Ubiquity and dominance of oxygenated species in organic aerosols in anthropogenically-influenced Northern Hemisphere midlatitudes. *Geophys. Res. Lett.* **34**, L13801 (2007).
25 Jimenez, J. L. *et al.* Evolution of organic aerosols in the atmosphere. *Science* **326**, 1525-1529 (2009).
26 Robinson, A. L. *et al.* Rethinking organic aerosols: semivolatile emissions and photochemical aging. *Science* **315**, 1259-1262 (2007).
27 Shrivastava, M. K., Lane, T. E., Donahue, N. M., Pandis, S. N. & Robinson, A. L. Effects of gas particle partitioning and aging of primary emissions on urban and regional organic aerosol concentrations. *J. Geophys. Res.* **113**, D18301 (2008).
28 Wang, T. *et al.* Air quality during the 2008 Beijing Olympics: secondary pollutants and regional impact. *Atmos. Chem. Phys.* **10**, 7603-7615 (2010).
29 Weber, R. J. *et al.* A study of secondary organic aerosol formation in the anthropogenic-influenced southeastern United States. *J. Geophys. Res. Atmos.* **112** (2007).
30 Gurjar, B. R., Butler, T. M., Lawrence, M. G. & Lelieveld, J. Evaluation of emissions and air quality in megacities. *Atmos. Environ.* **42**, 1593-1606 (2008).
31 Molina, L. T. & Molina, M. J. *Air Quality in the Mexico Megacity: An Integrated Assessment*. (Kluwer Academic Publishers, 2002).

32 Mage, D. *et al.* Urban air pollution in megacities of the world. *Atmos. Environ.* **30**, 681-686 (1996).
33 Molina, M. J. & Molina, L. T. Megacities and atmospheric pollution. *J. Air Waste Manage. Assoc.* **54**, 644-680 (2004).
34 Li, C. *et al.* Trends in chemical composition of global and regional population-weighted fine particulate matter estimated for 25 years. *Environ. Sci. Technol.* **51**, 11185-11195 (2017).
35 Health Effects Institute International Scientific Oversight Committee. Outdoor Air Pollution and Health in the Developing Countries of Asia: A Comprehensive Review. Special Report 18. (Health Effects Institute, Boston, MA, 2010).
36 Grossman, G. M. & Krueger, A. B. Economic growth and the environment. *The Quarterly Journal of Economics* **110**, 353-377 (1995).
37 Stern, D. I. The rise and fall of the Environmental Kuznets Curve. *World Development* **32**, 1419-1439 (2004).
38 Anenberg, S. C. *et al.* Particulate matter-attributable mortality and relationships with carbon dioxide in 250 urban areas worldwide. *Scientific Reports* **9**, 11552 (2019).
39 Pope, C. A., Ezzati, M. & Dockery, D. W. Fine-particulate air pollution and life expectancy in the United States. *N. Engl. J. Med.* **360**, 376-386 (2009).
40 Rich, D. Q. Accountability studies of air pollution and health effects: lessons learned and recommendations for future natural experiment opportunities. *Environ. Int.* **100**, 62-78 (2017).
41 Brauer, M. *et al.* Examination of monitoring approaches for ambient air pollution: A case study for India. *Atmos. Environ.* **216**, 116940 (2019).
42 Watts, M. Cities spearhead climate action. *Nat. Clim. Change* **7**, 537-538 (2017).
43 Acuto, M. The new climate leaders? *Review of International Studies* **39**, 835-857 (2013).
44 Ganguly, T., Selvaraj, K. L. & Guttikunda, S. K. National Clean Air Programme (NCAP) for Indian cities: Review and outlook of clean air action plans. *Atmos. Env. X* **8**, 100096 (2020).
45 *U.S.-Canada Air Quality Agreement*, <https://www.epa.gov/airmarkets/us-canada-air-quality-agreement> (1991).
46 United Nations. Convention on long-range transboundary air pollution. (1983).

Methods

Characterizing the global distribution and evolution of ambient $PM_{2.5}$ concentrations in cities globally is constrained by two factors: (i) the widespread absence of in-situ $PM_{2.5}$ measurements in most urban areas, especially in lower-income countries (Extended Data Figure 1); and (ii) the absence of a consistent long-term observational record of $PM_{2.5}$ in the many cities that have recently begun to monitor $PM_{2.5}$. To estimate $PM_{2.5}$ concentration time series for worldwide cities, we combined two key datasets, described briefly here and in detail below. First, we employ a dataset[14] recently developed by members of this group and others that estimates a 20-year time series (1998-2018) of annual-average $PM_{2.5}$ concentration using a combination of satellite remote sensing of aerosol optical depth (AOD) and modeled and observational constraints. Data are available for all major areas of the earth's land mass, gridded at 0.01º × 0.01º resolution, comparable to 1 km at mid-latitudes. We then obtained a comprehensive dataset of the world's major urban centers – the Universe of Cities dataset[11,12,47] – which enumerates 4231 worldwide urban areas ("cities") that had year-2010 populations greater than 100,000, accounting for ~70% of the global urban population in that year. Next, we developed a simple geospatial routine for estimating urban-average $PM_{2.5}$ concentrations for each of these 4231 cities using the gridded global dataset and validated these estimates against a global collection of in-situ $PM_{2.5}$ observations maintained by the World Health Organization.[10] Finally, we conducted trend analyses to characterize the time evolution of ambient $PM_{2.5}$ in cities and regions around the world.

Datasets

Global gridded $PM_{2.5}$ dataset

We use here a global time series of ground level annual-average $PM_{2.5}$ for the years 1998-2018 recently developed by Hammer et al. (2020).[14] This dataset is the latest refinement of a global gridded $PM_{2.5}$ product developed by van Donkelaar et al. over the past decade.[15,48] We provide here an overview of those methods and refer the reader to Hammer et al. (2020) and references therein for a full description. First, daily overpass aerosol optical depth (AOD) measurements are acquired from four satellite instruments (MODIS-Terra [operational 2000-present] and MODIS-Aqua [2002- present], MISR [2000 – present], and SeaWiFS [1997-2010]). A detailed summary of the specific retrieval algorithms used for each instrument is presented in Hammer et al. (2020). This dataset incorporates several recent refinements to the AOD retrievals for the individual instruments, including the MAIAC (Multi-Angle Implementation of Atmospheric Correction) algorithm[49] that provides AOD at a spatial resolution of 1 km globally for the entire MODIS record. Next, the individual daily remotely sensed AOD products are calibrated to a network of high-accuracy ground-based sun photometer AOD observations from the AERONET (Aerosol Robotic Network) system. Following calibration, the individual daily AOD products are combined into a single product based on a weighted average that most strongly emphasizes the AOD data sources with the best agreement with nearby AERONET sites. This combined satellite AOD product is highly consistent with AERONET observational constraints (e.g., for 638 monthly-averaged observations in 2015, $R^2 = 0.84$, slope = 0.97).[14]

To estimate surface $PM_{2.5}$ concentrations from satellite observations of the columnar AOD (AOD_{SAT}), Hammer et al. simulate the local and temporally coincident ratio of these two properties ($\eta = PM_{2.5,SIM} / AOD_{SIM}$) , such that:

$$PM_{2.5} = \eta \times AOD_{SAT}$$

The η parameter[15] is spatiotemporally variable, and depends on factors including aerosol composition, aerosol size, relative humidity, diurnal variation, and the vertical atmospheric profile of aerosol extinction. Hammer et al. (2020) employ v11-01 of the GEOS-Chem chemical transport model (http://geos-chem.org) and meteorological data from the MERRA-2 assimilated reanalysis to simulate temporally coincident surfaces of η globally from 1998-2018. The GEOS-Chem simulation incorporated 47 vertical layers at a global grid resolution of 2º×2.5º, with a nested resolution of 0.5º×0.625º over Europe, North America, and China. The Hammer et al. dataset includes several refinements to the GEOS-Chem simulations relative to earlier datasets[15,48] including: (i) improved parameterizations for secondary organic aerosol and dust; (ii) updated anthropogenic emissions inventories for the US, Europe, China, India, and elsewhere in Asia, and (iii) increased global coverage at finer resolution for biomass burning and crustal dust emissions.

The $PM_{2.5}$ estimates produced with Equation 1 above are referred to as a geophysical estimate, given that they are derived strictly from observational constraints and a mechanistic simulation. To evaluate the geophysical model, Hammer et al. (2020) employed the latest version of the World Health Organization ambient air quality database, which provides a comprehensive and harmonized global dataset of all available annual-average $PM_{2.5}$ measurements from scientific or regulatory-grade instruments from 2010 onwards. Hammer et al. (2020) selected from this dataset a total of ~23,000 measurements in 66 countries that had 75% or greater data coverage in their given measurement year for validation of the annual-average geophysical $PM_{2.5}$ product. In recent measurement years, approximately 3500-4000 sites are available for evaluation of the dataset, reflecting expansion of global monitoring coverage in China, India, and other lower-income countries. The annual mean geophysical product is consistent with ground-

based monitors, with R^2 = 0.81 and slope = 0.90 for 2015. Few regions of the world have consistent, long-term datasets available for evaluating the *trends* of the geophysical product. For the eastern US, US EPA monitoring data are available for evaluating the entire 1998-2018 period, and show excellent agreement in monthly and annual $PM_{2.5}$ trends.[14] The historical record of $PM_{2.5}$ is considerably shorter for data in Europe and China, but trends are broadly consistent and agree to within the uncertainty bounds of the dataset.

To further improve the fidelity of the AOD product, Hammer et al. (2020) develop a "hybrid" dataset where the geophysical $PM_{2.5}$ data are statistically fused to the global dataset of in-situ observations by means of geographically weighted regression (GWR). Briefly, the GWR bias correction is parameterized to minimize the difference between in-situ annual-average $PM_{2.5}$ measurements and the geophysical $PM_{2.5}$ surface concentrations at monitor locations. Predictor variables for the GWR are properties that are associated with uncertainties in η: fine-scale topography, simulated aerosol composition (mineral dust, sulfate, nitrate, ammonium, organic carbon), and urban land cover. Application of the GWR improves the performance of the hybrid model relative to the geophysical model (10-fold cross validation R^2 0.90-0.92, slope 0.91-0.97 for years 2014-2016). Overall, geophysical $PM_{2.5}$ is still the principal driver of the hybrid $PM_{2.5}$ surface, with statistical fusion explaining only 11% of the variance in the $PM_{2.5}$ surface.[14] Here, for our core estimates of urban $PM_{2.5}$, we rely on the hybrid $PM_{2.5}$ surface, and in sensitivity analyses consider how our conclusions would be affected if we had instead employed the geophysical $PM_{2.5}$ surface.

Global data on urbanized areas

To characterize the global distribution of urban areas, we rely on a dataset developed by Angel et al. that seeks to produce a globally consistent description of the population and urban

form of human settlements.[11,12,50] The core Angel et al. dataset, termed the "Universe of Cities", provides information on year-1990, 2000, and 2010 populations for 4231 global urban areas, along with the geographic coordinates of the approximate center of each city, derived using global and national demographic datasets and constrained by satellite imagery. Herein, we follow the practice of Angel et al., and use the term "city" interchangeably with the more formalized concept of an urban area. For each urban area in the Universe of Cities, Angel et al. conducted quality assurance to ensure that population estimates refer to the urban agglomeration, rather than to individual administrative subunits, and similarly ensure that constituent cities / subunits are excluded as separate entries when part of a larger urban agglomeration. Overall, this dataset of cities > 100,000 people incorporates a year-2010 population of 2.49 billion urban inhabitants, roughly ~72% of the year-2010 global urban population estimated by the UN World Urbanization Prospects dataset.[13] For the purposes of analysis, we subdivide these cities into four groups (approximately quartiles) with nearly equal population: 0.1 – 0.4 M people (24%, N = 3073 cities), 0.4 –1.6 M people (26%, N = 890), 1.6 – 5.6 M people (25%, N = 215), and > 5.6 M people (25%, N = 53).

In addition to the full "Universe" of 4231 global urban areas, Angel et al. use a stratified sampling frame based on world region, income category, and city size to select 200 individual cities ("Atlas of Urban Expansion") for detailed time-series analysis. For each of these 200 cities, Angel et al. provide high-resolution GIS shapefiles that correspond to the urban boundaries over multiple time periods, including year-2010. Here, we employ the detailed data for these 200 cities for developing and validating a geospatial data analysis method that we subsequently applied to all 4231 worldwide urban areas.

To estimate regional urban population growth between 1998 and 2018 at finer temporal resolution than the year-2000 and year-2010 data available for individual cities from Angel et al., we performed the following routine. First, using city-specific population estimates for years 2000 and 2010, we derived annual population estimates between 1998 and 2010 using the decadal-average population growth rate for 2000-2010. For years 2010 onward, city-specific population estimates were not available. For each country, we obtained estimated national growth rates in urban population for the periods 2010-2015 and 2015-2020 from the UN World Urbanization Prospects database[13] and applied these growth rates uniformly to each city in a country. Population estimates for individual cities may therefore be substantially uncertain post-2010, but we expect the overall trends in combined urban population for groupings of many cities to reflect well the UN urbanization estimates.

Estimating urban $PM_{2.5}$ from gridded data

To estimate urban $PM_{2.5}$ from gridded data, we employed two approaches. First, for the 200 individual cities of Angel et al.,[11] we used detailed urban boundary data for circa-2010 to estimate an area-weighted $PM_{2.5}$ concentration from the gridded dataset. Specifically, we assign each grid cell that is partially or fully intersected by a given city's urban boundary a weighting factor in proportion to the fraction of that grid cell's area encompassed by the urban boundary. Given the relatively high spatial resolution of the gridded $PM_{2.5}$ data (0.01º, ~ 1 km), the footprints of even the smallest and most compact cities in the dataset (~10 km^2 urbanized land) intersect dozens of pixels, while there are hundreds to tens of thousands of pixels in the larger cities evaluated here.

Second, we consider a highly simplified approach, wherein $PM_{2.5}$ is estimated on the basis of a circular buffer around each city's centroid. For this latter approach, we sized each city's

circular buffer to correspond to the mean urbanized land area for the full set of cities in its population quartile (respectively 125, 265, 951 and 2190 km^2; radii of 6.3, 9.2, 17.4 and 26.4 km). For the set of 200 cities, the simplified circular approach estimates the area-weighted concentrations using urbanized boundaries with remarkably high fidelity: $R^2 = 0.997$, slope = 1.001, normalized mean absolute error 2.3%, normalized root-mean-square error (NRMSE) 3.9%, and mean fractional bias -0.8% (see Extended Data Figure 3a). We speculate that this simplified circular buffer approach performs well for many cities because (i) the spatial gradients of $PM_{2.5}$ across an urban region are generally moderate (varying by tens of percent, not by multiples), given the importance of secondary/regional $PM_{2.5}$; (ii) both spatial analysis methods involve smoothing over hundreds to thousands of grid pixels; and (iii) a crudely drawn circle roughly approximates the urban form of many cities. Given the success of this simplified method, we then applied the circular buffer approach to all 4231 global urban areas in the Universe of Cities dataset.

Evaluation of urban $PM_{2.5}$ estimates

To evaluate the performance our urban $PM_{2.5}$ dataset in estimating in-situ measurements of ambient concentration, we matched the cities in our dataset to the World Health Organization (WHO) ambient air quality dataset. First, following Hammer et al., we restricted the dataset to include only the measurement data with >75% temporal coverage for a given year. Then, for each city, we identified (i) all monitors available within a 30 km radius of the city center and (ii) all monitors available within the specified radius of the city center that we used for analyzing gridded $PM_{2.5}$ concentrations (6.3 – 25.4 km, see above). Overall, 1387 cities (33%) had valid monitoring data from sites within 30 km of the city center, and 1007 cities (24%) in 66 countries had monitors within the narrower 6.3-26.4 buffer radius we used for analyzing the gridded $PM_{2.5}$

463 data. For this latter set of cities, there were ~12,600 valid measurements, reflecting multiple
464 monitors per city in multiple years. We then analyzed the relationship between the in-situ
465 measurement and remotely sensed $PM_{2.5}$ data sets in two ways. First, we considered the
466 correlation between individual monitoring sites' annual average $PM_{2.5}$ concentration and the
467 corresponding year's $PM_{2.5}$ estimate. Second, to reduce the monitor-to-monitor differences in
468 cities with multiple monitors, we evaluated the relationship between the median concentration
469 computed over all measurement sites in each city for a given year, and our corresponding
470 estimate for the same year. For this second approach, our dataset was reduced to ~5600
471 measurements. In each case, we employed orthogonal distance (Deming) regression. Regression
472 results were broadly similar for both analysis approaches for the monitoring data, as illustrated in
473 Extended Data Figure 3. The city-averaged approach estimated available measurements of
474 ambient $PM_{2.5}$ with good fidelity: $R^2 = 0.91$, normalized mean absolute error (NMAE)= 16%,
475 normalized root-mean-squared error (NRMSE) = 26%, with regression slope = 0.91 (Extended
476 Data Figure 3). As an additional test of our results, we considered an alternative approach to the
477 hybrid $PM_{2.5}$ dataset, where the GWR correction was applied based on an out-of-sample
478 prediction from the 10-fold cross-validation scheme of Hammer et al. This approach ensures that
479 local monitoring information is withheld from our hybrid model estimates while still maintaining
480 the overall benefit of the GWR correction. Here, evaluation results were nearly identical. Thus,
481 we can conclude that our product estimates urban-average $PM_{2.5}$ with moderate to high precision,
482 at least on the basis of the extant measurement datasets. Consider for context that our precision
483 metrics (~15-25%) are comparable in magnitude to the typical level of spatial variation of $PM_{2.5}$
484 within a city, whereas variation in $PM_{2.5}$ concentrations among cities within many countries can
485 span a factor of 2 to 5. Of course, we anticipate that the GWR correction scheme would benefit

from additional monitoring data, especially for regions with comparatively few urban measurements. As shown in Extended Data Figure 3b, we observe somewhat greater dispersion in our estimates for cities in the low-income countries. This result may arise from a combination of factors: (i) fewer data available to train the GWR in regions with limited in-situ monitoring, (ii) fewer monitors per city, (iii) the difficulty of siting "background" ambient monitors at a distance from high-emitting pollution sources in dense low-income cities and (iv) QA/QC considerations in the monitoring data.[16]

Globally, we find that the population-weighted mean *urban* PM_{25} concentration is somewhat lower than the PWM $PM_{2.5}$ concentration for the entire global population (i.e., urban + non-urban combined). For 2015, using the core dataset of Hammer et al.,[14] we find a global PWM $PM_{2.5}$ concentration of 38.6 $\mu g\ m^{-3}$, as compared with an urban PWM concentration 34.9 $\mu g\ m^{-3}$. This counter-intuitive result arises because of regional differences in the urban share of the population: on average, more polluted regions of the world are less urbanized, and therefore contribute less urban population to the PWM. Controlling for regional differences in urban population share (i.e., if the regional distribution of urban population matched the total population), our dataset would find hypothetical urban PWM concentrations of ~39-40 $\mu g\ m^{-3}$ for 2015, or ~1-3% higher than the global PWM.

Trend analyses

To characterize the evolution of $PM_{2.5}$ for the 1998 to 2018 period, we employed a least-squares fitting approach to quantify temporal trends and their associated statistical significance. We first considered three time-windows for trend analyses: the 1998-2008 and 2008-2018 decades, and the combined two-decade period. In addition, given the sharp inflection point in $PM_{2.5}$ trends over East Asia beginning in 2011, we considered 2011 as an alternative breakpoint

509 in our analysis for cities in East Asia. For each city and evaluation period, we fit two simple
510 models: a linear model (concentration trend in μg m^{-3} y^{-1}) and an exponential model
511 (concentration trend in % y^{-1}). For each model and city, we report the trend coefficient and the
512 coefficient of determination (R^2) and *p*-value of the regression relationship. Given the large
513 dynamic range in global $PM_{2.5}$ concentrations, we emphasize the percentage change trends to
514 facilitate global comparisons in our key figures (Figure 1, Extended Data Figure 5), and include
515 additional reference to absolute concentration trends in our discussion. While the selection of an
516 evaluation period in any trend analysis ultimately involves an analyst's discretion, an advantage
517 of reporting trends – rather than the change in concentration between a pair of two specific
518 annual point estimates – is that multi-year analyses are less sensitive to interannual variability.[14]

519 ## Spatial analysis

520 To characterize the spatial relationship of $PM_{2.5}$ between urban areas and the regions that
521 surround each city, we conducted the following distance decay analysis. For each city in the
522 dataset, we constructed a series of 10-km wide annular buffers at sequentially increasing
523 distances from the city center: 5-15 km, 15-25 km, 25-35 km, … , 295 – 305 km. Then, for each
524 annular buffer, we computed the area-weighted average $PM_{2.5}$ concentration over all grid cells in
525 the buffer. As a sensitivity case to our core analysis, excluded those grid cells that included other
526 nearby cities when computing these spatial averages. For most cities, concentrations in each ring
527 decreased monotonically with increasing distance from the city center. Following the method of
528 Karner et al.[51] for distance-decay analyses, we normalized each city's decay profile to the city-
529 center concentration, and then averaged these individual profiles over all cities within the four
530 population size quartiles (Figure 3). Through the sensitivity case described above, we determined

that, on average, the distance-decay relationship was not strongly sensitive to the contribution of other nearby cities.

Methods References

10 World Health Organization. *WHO Global Ambient Air Quality Database (Update 2020)*. (WHO, 2020).

11 Angel, S. *et al.* Atlas of urban expansion—2016 edition. *Areas and densities. Cambridge, MA: NYU Urban Expansion Program at New York University, UN-Habitat, and the Lincoln Institute of Land Policy* (2016).

12 Angel, S., Parent, J., Civco, D. L., Blei, A. & Potere, D. The dimensions of global urban expansion: Estimates and projections for all countries, 2000-2050. *Prog. Plann.* **75**, 53-107 (2011).

13 United Nations; Department of Economic and Social Affairs; Population Division. *World Urbanization Prospects: The 2018 Revision*. (2018).

14 Hammer, M. S. *et al.* Global estimates and long-term trends of fine particulate matter concentrations (1998–2018). *Environ. Sci. Technol.* **54**, 7879-7890 (2020).

15 van Donkelaar, A. *et al.* Global estimates of ambient fine particulate matter concentrations from satellite-based aerosol optical depth: development and application. *Environ. Health Persp.* **118**, 847-855 (2010).

16 Schwela, D. H. & Haq, G. Strengths and weaknesses of the WHO Urban Air Pollutant Database. *Aerosol Air Qual. Res.* **20**, 1026-1037 (2020).

47 Angel, S., Blei, A. M., Civco, D. L. & Parent, J. *Atlas of urban expansion*. (Lincoln Institute of Land Policy Cambridge, MA, 2012).

48 van Donkelaar, A. *et al.* Global estimates of fine particulate matter using a combined geophysical-statistical method with information from satellites, models, and monitors. *Environ. Sci. Technol.* **50**, 3762-3772 (2016).

49 Lyapustin, A., Wang, Y., Korkin, S. & Huang, D. MODIS Collection 6 MAIAC algorithm. *Atmos. Meas. Tech.* **11**, 5741-5765 (2018).

50 Angel, S. *et al.* The Dynamics of Global Urban Expansion. (Transport and Urban Development Department, World Bank, Washington, DC, 2005).

51 Karner, A. A., Eisinger, D. S. & Niemeier, D. A. Near-roadway air quality: Synthesizing the findings from real-world data. *Environ. Sci. Technol.* **44**, 5334-5344 (2010).

Author contributions

Study design: JSA, SS, SEC, RVM. Data generation: MH, AVD, RVM, JSA. Data analysis: JSA, SS, SEC. Data interpretation: JSA, SS, SEC, MH, RVM, SCA, MB. Writing: all authors.

Data availability

An archival library of our input data and results is available at DOI:10.5281/zenodo.4777367. The data underlying each figure can be generated by the replication code presented in this repository.

Code availability

All analysis and data visualization code is available at DOI:10.5281/zenodo.4777367, along with supporting documentation.

Supplemental information

City-level $PM_{2.5}$ data and associated trend results for years 1998-2018 are available in spreadsheet format in the SI file.

Additional information

Correspondence and requests for materials should be addressed to Joshua Apte, apte@berkeley.edu. Reprints and permissions information is available at www.nature.com/reprints.

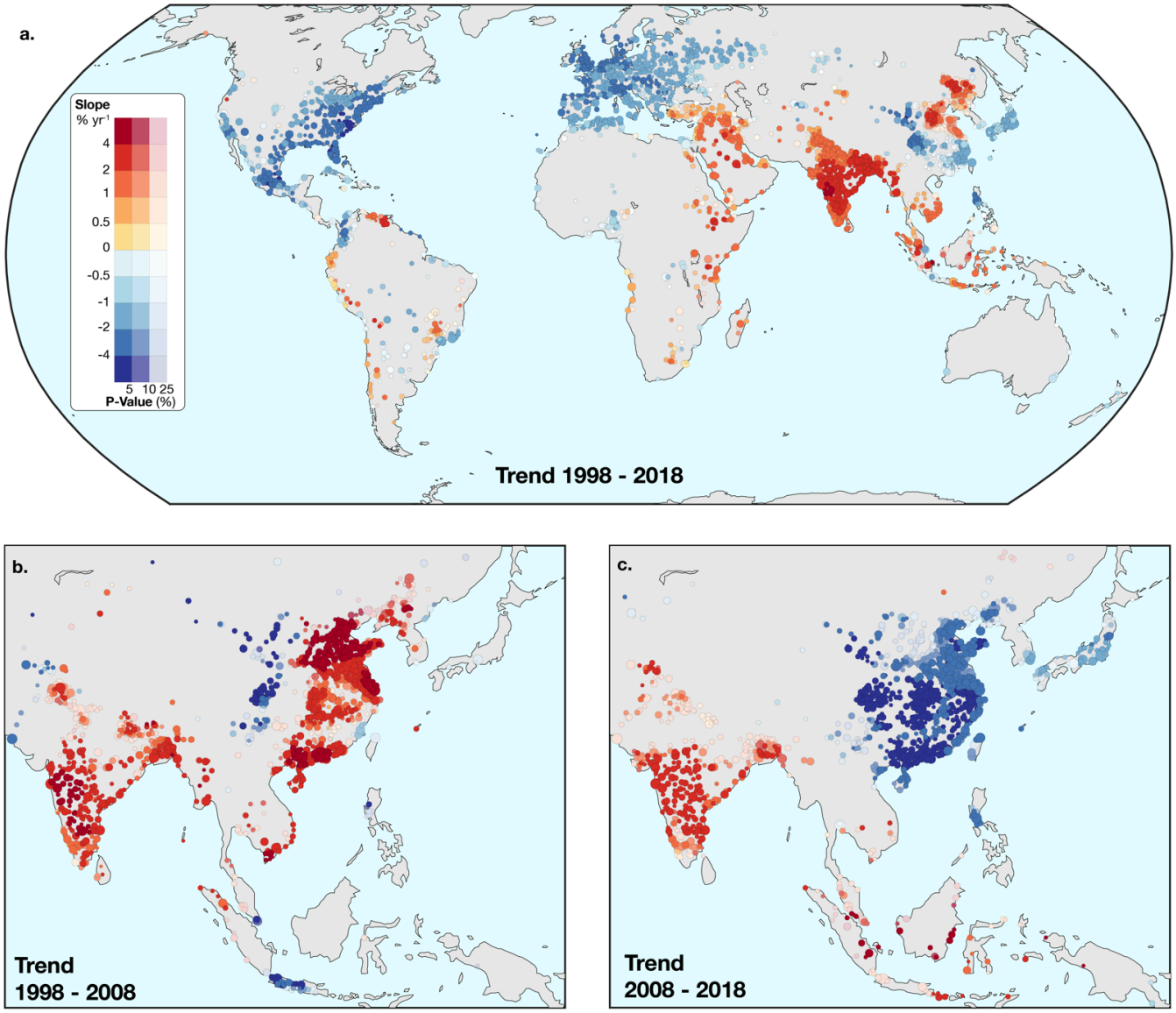

Figure 1. Best-fit trends of annual percentage change in urban $PM_{2.5}$ for **a.**1998-2018, **b.** 1998-2008, and **c.** 2008-2018. Only cities for which the regression *p*-value < 0.25 are plotted, with more rapid $PM_{2.5}$ changes and higher levels of statistical significance plotted with more intense colors. Compare **b** vs. **c** to note the sharp reversal in the trend of $PM_{2.5}$ in urban China between the first and second decades of the dataset. Markers proportional to logarithm of city population. Extended Data Figure 5 presents detailed trend analyses for several world regions.

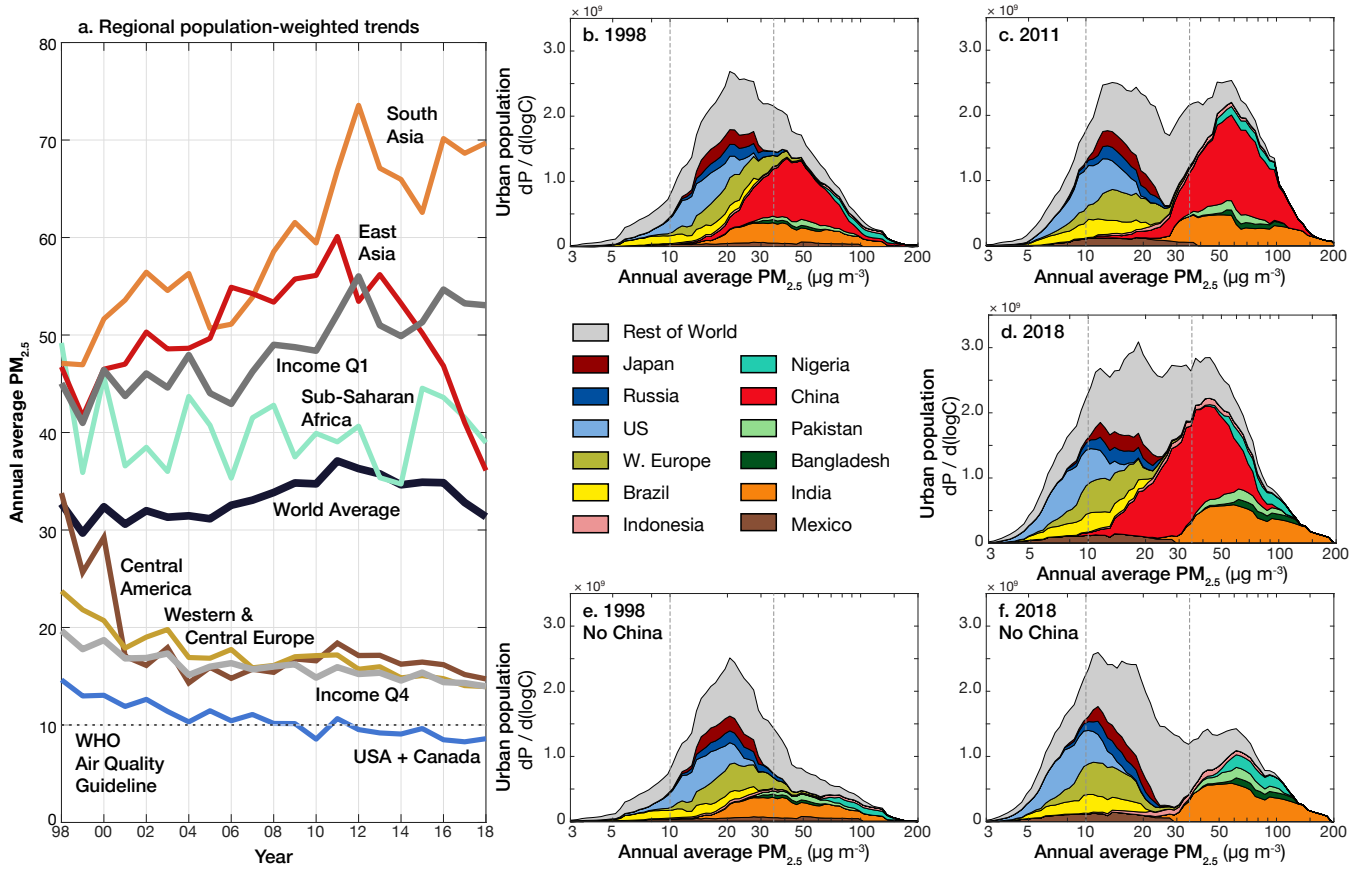

Figure 2. **Regional trends in urban $PM_{2.5}$ air quality exhibit divergence between higher and lower-income countries. a**. Trends in population-weighted mean urban $PM_{2.5}$ for selected major world regions 1998-2018, illustrating the contrasting trends between East Asia and South Asia after 2011. Concentrations diverged increasingly between cities in the lowest and highest income quartiles (Q1 and Q4, based on year-2018 GDP per capita < $3200 or > $16,400) over this two-decade period. **b-d.** Population-concentration distributions for 1998, 2011, and 2018 for the world's largest countries. Plots illustrate the distribution of the national urban population over the $PM_{2.5}$ concentration spectrum for individual countries, with axes scaled to present equal populations with equal plotted areas. Panels **b-d** illustrate an increasing divergence in the concentration distributions between high-income and lower-income countries, and reveal the rapid shift towards lower $PM_{2.5}$ in China post-2011. Panels **e-f** plot all world countries except China, revealing how the distribution of urban $PM_{2.5}$ has become strongly bimodal, separating less polluted middle- and high-income countries from more polluted lower-income countries. Despite increasing global divergence in population weighted $PM_{2.5}$, the global population-weighted $PM_{2.5}$ concentrations **(a)** have varied by less than 20% over the full time period.

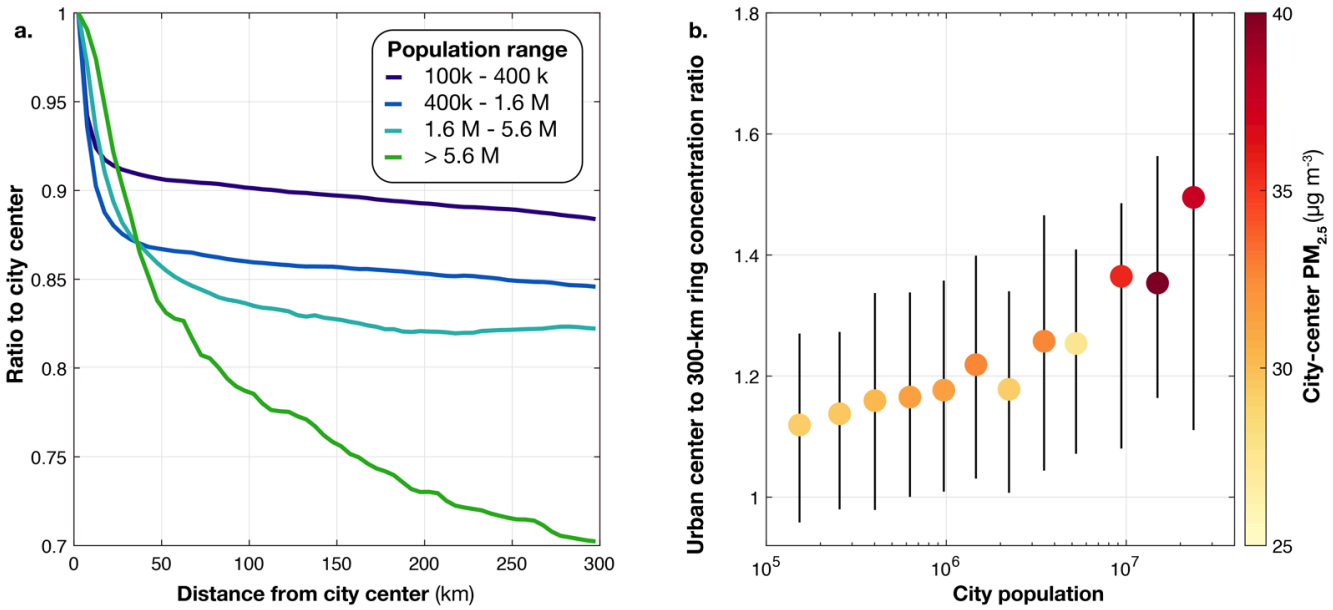

Figure 3. Urban $PM_{2.5}$ concentrations are modestly elevated above the regional background. a. Isotropic radial distance-decay functions for urban $PM_{2.5}$ normalized to the city-center concentration. Lines show geometric mean decay profile for four groups of increasing city size, each with ~25% of global urban population. **b.** Distributions of the ratio of city-center $PM_{2.5}$ to concentrations in the 300±5 km distance band for cities of increasing size. Global distribution of city population is divided into 12 equal-population groupings, with geometric mean and 25th-75th percentile range of this ratio plotted for each grouping. Marker color shows population-weighted mean $PM_{2.5}$ concentration for each city size grouping.

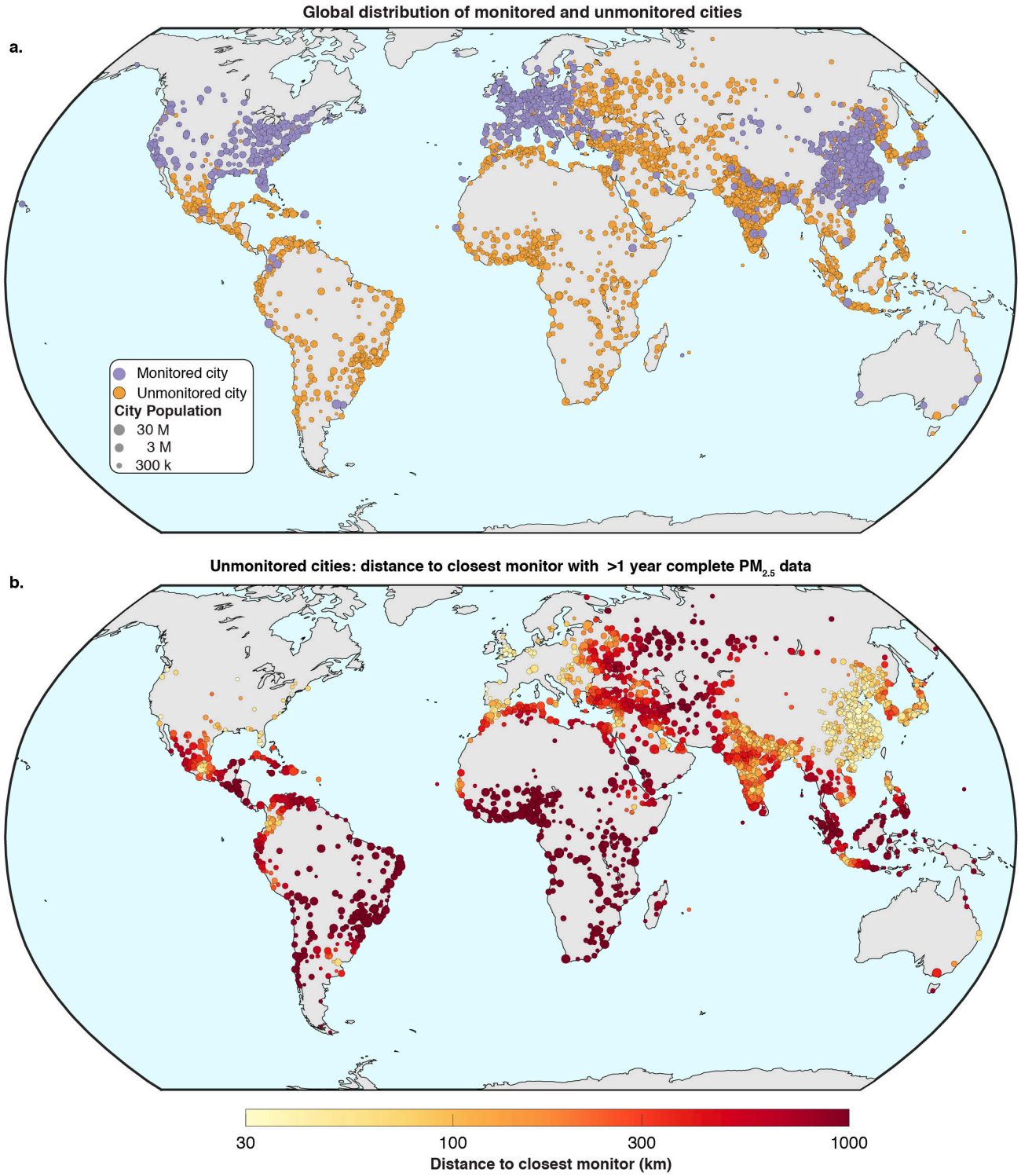

615
616 **Extended Data Figure 1 – Global in-situ $PM_{2.5}$ monitoring gaps**. **a.** Cities in the 2020 WHO
617 Urban Air Quality Database with and without monitors, defined here as at least one valid (>75%
618 complete data) annual-average $PM_{2.5}$ measurement present within 30 km of the city center. **b.**
619 For cities without valid $PM_{2.5}$ monitoring data, the distance to the closest monitor in the WHO
620 dataset with at least one year of valid $PM_{2.5}$ data.

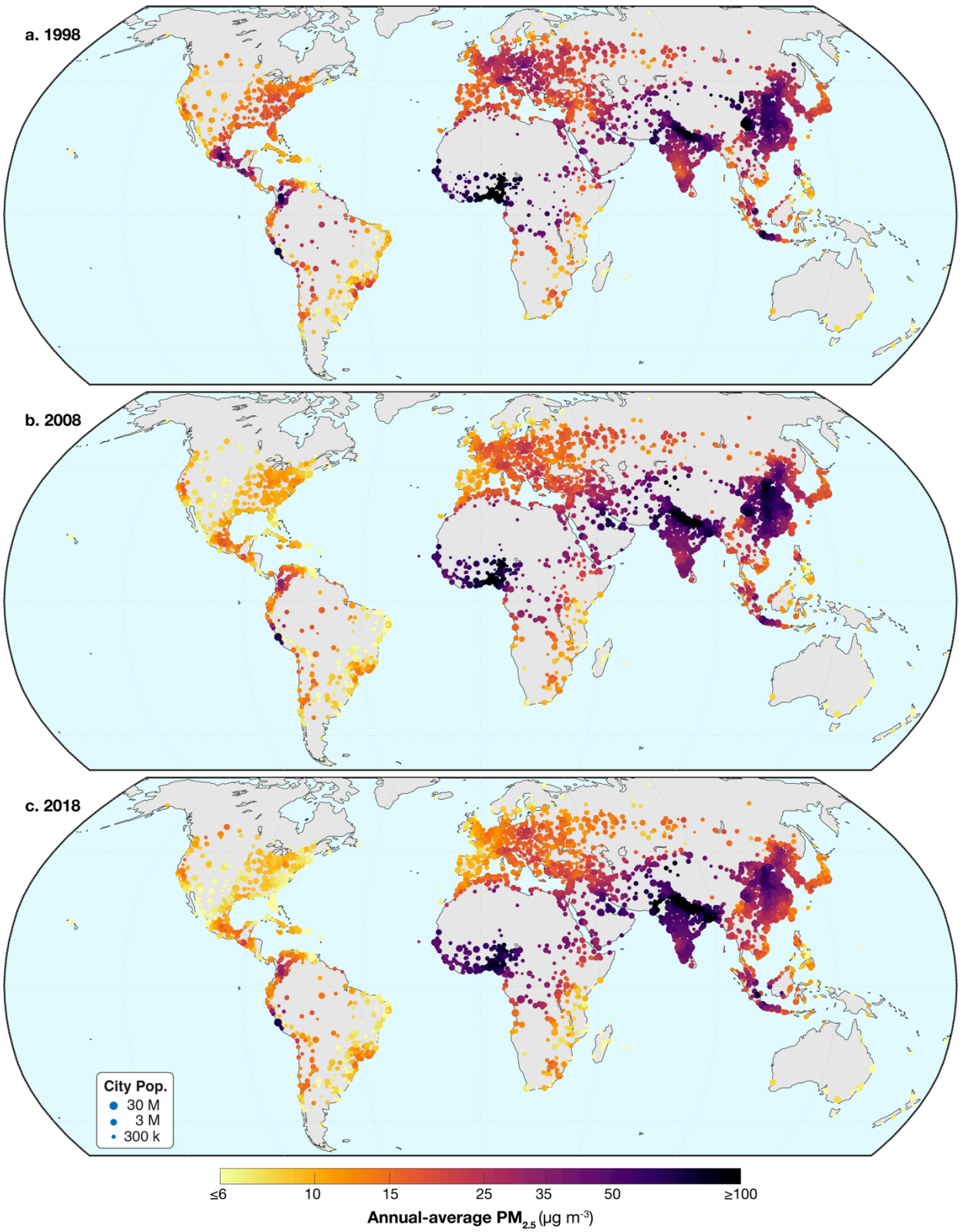

Extended Data Figure 2. Annual-average $PM_{2.5}$ estimates for 4231 world cities for **a.** 1998, **b.** 2008 and **c.** 2018. Logarithmic color scale represents ~2^{nd} – 98^{th} percentiles of the year-2018 population weighted concentration distribution.

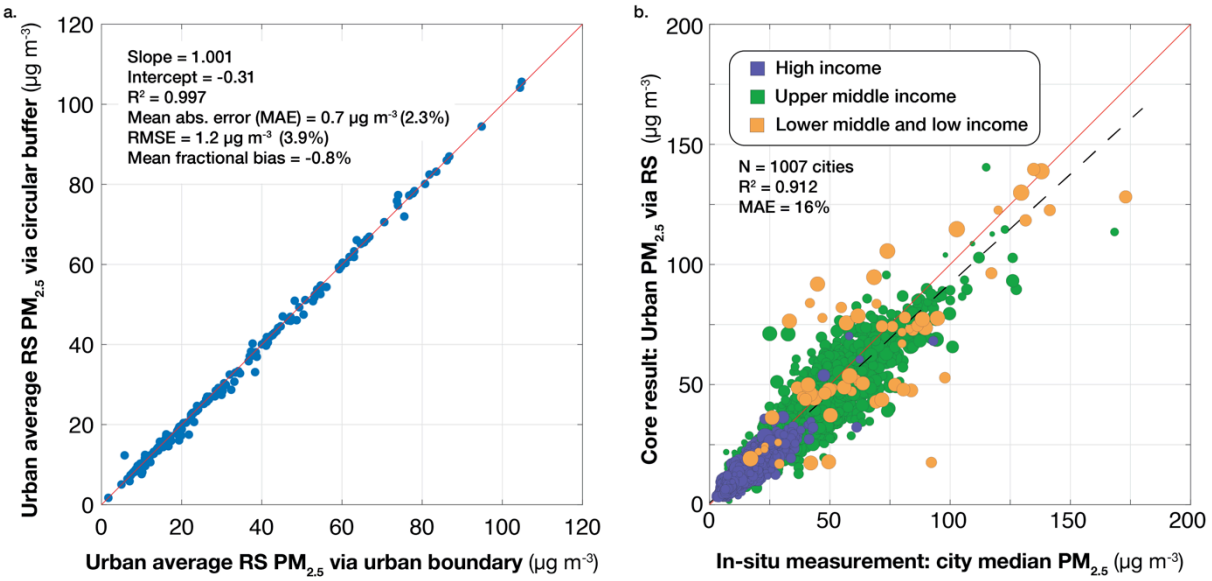

c.

	(i) Annual median of all monitors by city	(ii) Alternative approach: Individual Monitors
N data points (city-years [i] or monitor-years [ii])	5626	12588
N cities	1007	1007
Total year-2010 Pop (billions)	1.20	1.18
% of urban dataset population	48%	48%
R-Squared	0.91	0.91
Normalized mean absolute error (NMAE)	15.8%	15.9%
Normalized root mean squared error (NRMSE)	26.0%	20.9%
Normalized Mean Bias	-5.3%	-6.3%
Mean at monitors (µg/m3)	22.8	28.4
Mean of city estimates	21.6	26.6
Orthogonal distance regression slope	0.78	1.08
Orthogonal distance regression intercept (µg/m3)	0.91	0.90

Extended Data Figure 3. Validation statistics for estimating urban $PM_{2.5}$ via the satellite remote sensing (RS) method. a. Validation of circular buffer approach for estimating urban-average $PM_{2.5}$ against a detailed urban boundary shapefile for a subset of 200 cities in the Universe of cities dataset. **b.** Scatterplot comparing the annual-median of available WHO $PM_{2.5}$ monitors with >75% data completeness with the corresponding core RS estimates of annual-average $PM_{2.5}$ estimate from this database. A total of 5626 annual-average estimates from 1998-2018 are available for 1007 cities with ~ 1.2 billion inhabitants. Dashed line indicates best-fit orthogonal distance regression relationship (R^2 = 0.91, slope 0.91). Marker proportional to logarithm of city population. **c.** Validation statistics comparing this analysis's core RS city annual-average estimates against (i) the median of all in-situ monitors in a city for each year and (ii) against annual average concentrations recorded at individual in-situ monitors in a city.

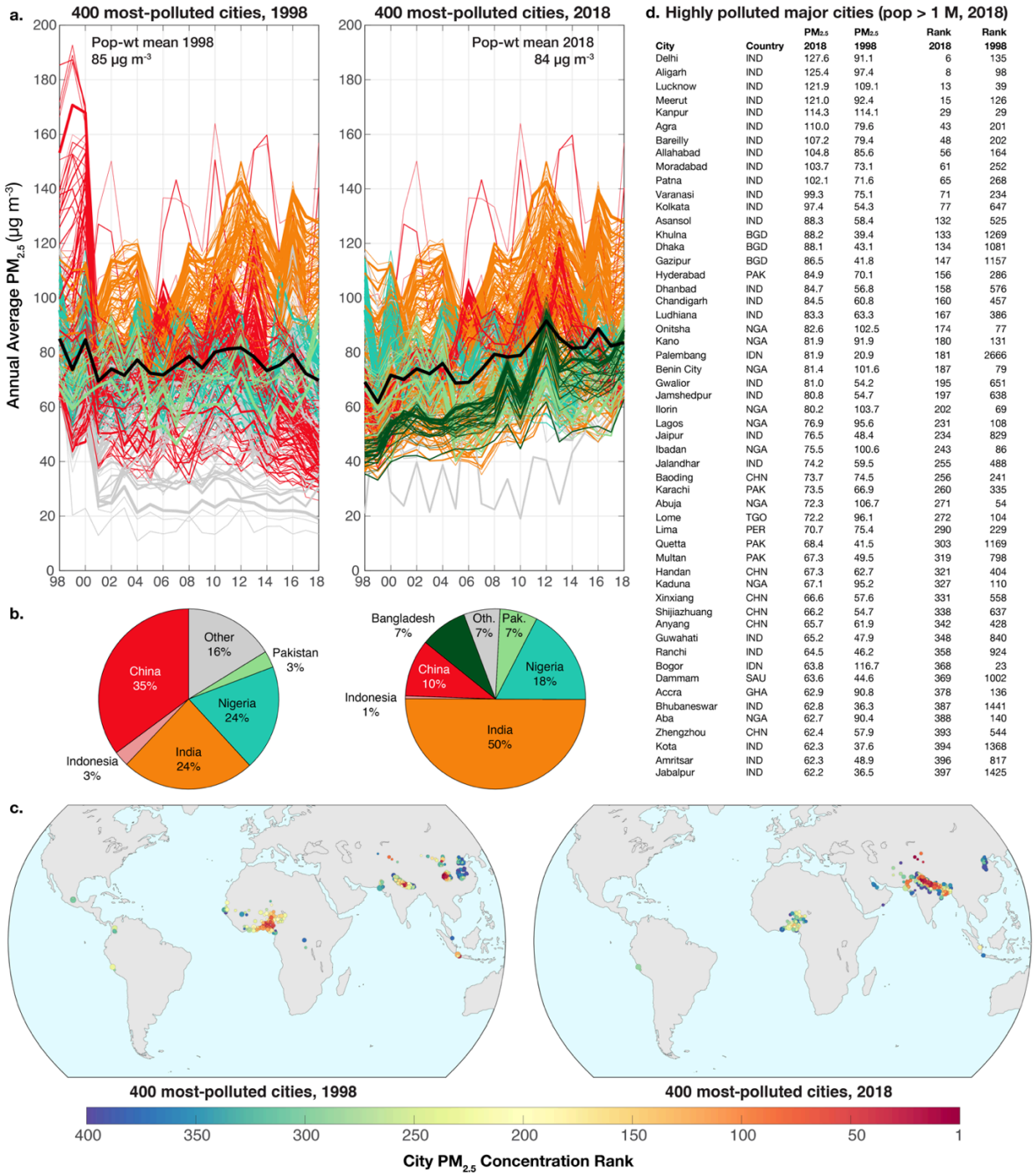

d. Highly polluted major cities (pop > 1 M, 2018)

City	Country	$PM_{2.5}$ 2018	$PM_{2.5}$ 1998	Rank 2018	Rank 1998
Delhi	IND	127.6	91.1	6	135
Aligarh	IND	125.4	97.4	8	98
Lucknow	IND	121.9	109.1	13	39
Meerut	IND	121.0	92.4	15	126
Kanpur	IND	114.3	114.1	29	29
Agra	IND	110.0	79.6	43	201
Bareilly	IND	107.2	79.4	48	202
Allahabad	IND	104.8	85.6	56	164
Moradabad	IND	103.7	73.1	61	252
Patna	IND	102.1	71.6	65	268
Varanasi	IND	99.3	75.1	71	234
Kolkata	IND	97.4	54.3	77	647
Asansol	IND	88.3	58.4	132	525
Khulna	BGD	88.2	39.4	133	1269
Dhaka	BGD	88.1	43.1	134	1081
Gazipur	BGD	86.5	41.8	147	1157
Hyderabad	PAK	84.9	70.1	156	286
Dhanbad	IND	84.7	56.8	158	576
Chandigarh	IND	84.5	60.8	160	457
Ludhiana	IND	83.3	63.3	167	386
Onitsha	NGA	82.6	102.5	174	77
Kano	NGA	81.9	91.9	180	131
Palembang	IDN	81.9	20.9	181	2666
Benin City	NGA	81.4	101.6	187	79
Gwalior	IND	81.0	54.2	195	651
Jamshedpur	IND	80.8	54.7	197	638
Ilorin	NGA	80.2	103.7	202	69
Lagos	NGA	76.9	95.6	231	108
Jaipur	IND	76.5	48.4	234	829
Ibadan	NGA	75.5	100.6	243	86
Jalandhar	IND	74.2	59.5	255	488
Baoding	CHN	73.7	74.5	256	241
Karachi	PAK	73.5	66.9	260	335
Abuja	NGA	72.3	106.7	271	54
Lome	TGO	72.2	96.1	272	104
Lima	PER	70.7	75.4	290	229
Quetta	PAK	68.4	41.5	303	1169
Multan	PAK	67.3	49.5	319	798
Handan	CHN	67.3	62.7	321	404
Kaduna	NGA	67.1	95.2	327	110
Xinxiang	CHN	66.6	57.6	331	558
Shijiazhuang	CHN	66.2	54.7	338	637
Anyang	CHN	65.7	61.9	342	428
Guwahati	IND	65.2	47.9	348	840
Ranchi	IND	64.5	46.2	358	924
Bogor	IDN	63.8	116.7	368	23
Dammam	SAU	63.6	44.6	369	1002
Accra	GHA	62.9	90.8	378	136
Bhubaneswar	IND	62.8	36.3	387	1441
Aba	NGA	62.7	90.4	388	140
Zhengzhou	CHN	62.4	57.9	393	544
Kota	IND	62.3	37.6	394	1368
Amritsar	IND	62.3	48.9	396	817
Jabalpur	IND	62.2	36.5	397	1425

Extended Data Figure 4. $PM_{2.5}$ trends in the world's most polluted cities. a. Time evolution of $PM_{2.5}$ for the 400 cities with the highest concentrations in 1998 and 2018, equivalent to the top decile of their respective distributions. Line width is proportional to the logarithm of urban population and colored by country (black line is pop-wt average). Plots **b-c** show the regional distribution and location of the most polluted cities in 1998 and 2018, illustrating in conjunction with **a** how most Chinese cities in the top decile in 1998 experienced substantial reduction in $PM_{2.5}$ by 2018, and were replaced mostly by increasingly polluted South Asian cities. Average $PM_{2.5}$ for the top decile of cities changed little between 1998 and 2018 (average ~ 85 μg m^{-3}). The 54 individual cities in the top decile for 2018 with population > 1 M are listed in **d**, with rankings pertaining to the overall distribution of 4231 cities**.**

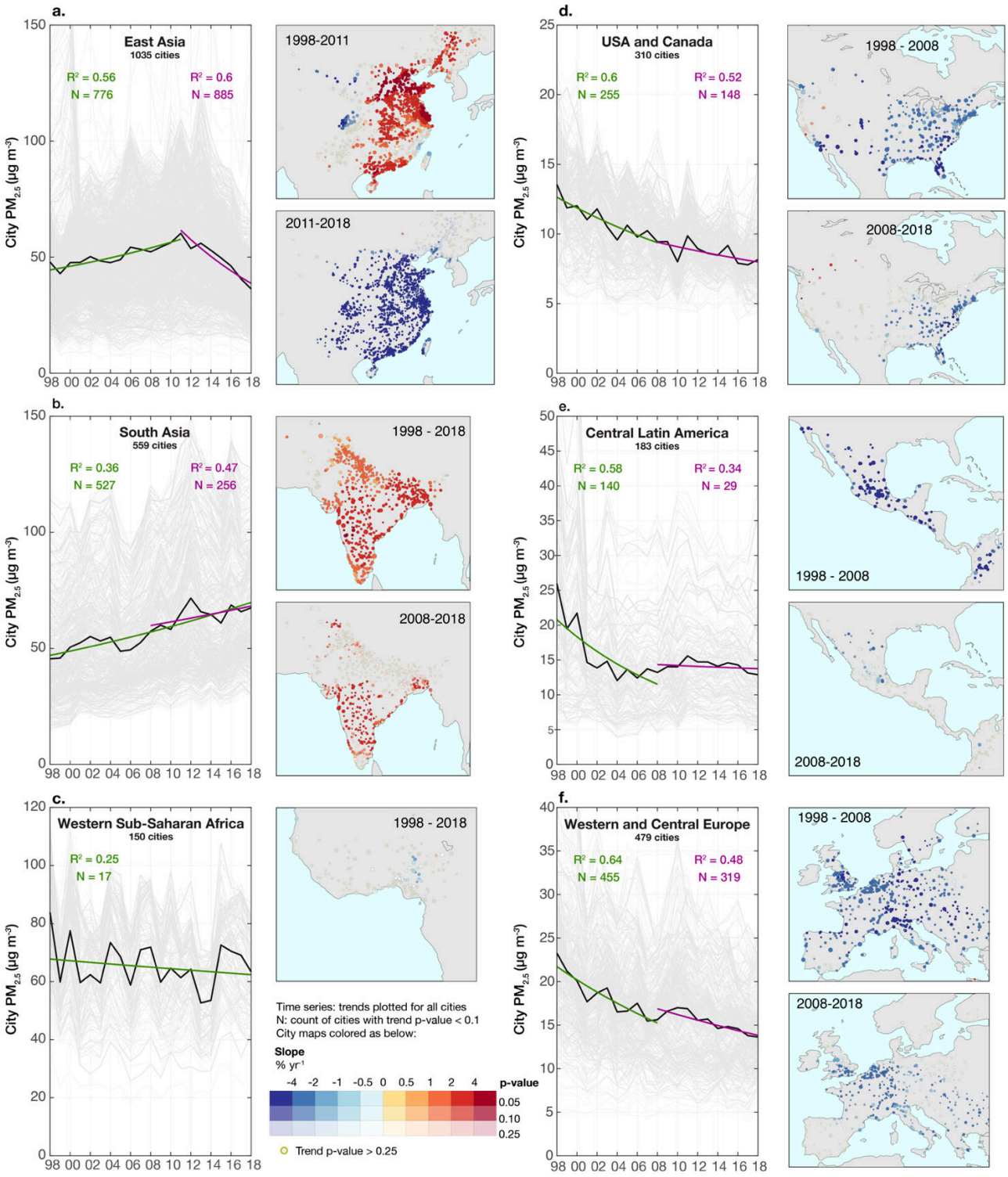

Extended Data Figure 5 – $PM_{2.5}$ trends 1998-2018 for six major world regions. Annual evolution of $PM_{2.5}$ for all individual cities in each region plotted as a grey line with width proportional to the logarithm of population. Best-fit annual-percentage-change trends are computed for each city for individual time periods, and plotted and mapped for cities where the regression slope $p < 0.1$. Time trends are either plotted for two individual decades (1998-2008, 2008-2018), or for alternative time periods where a marked inflection point existed. Trend plots display the mean time evolution for all cities (black line), and for those N cities with regression $p < 0.1$, the mean fitted time trend and accompanying R^2.